# Boundary layer flows over deforming surfaces

N. Hanevy,[1] J. Ferguson,[1] P. M. J. Trevelyan,[1] and P. T. Griffiths[1]

*Department of Applied Mathematics and Data Science, Aston University, Birmingham, B4 7ET, UK*

(*Electronic mail: nhane22@aston.ac.uk)

(Dated: 06 May 2024)

In this paper a formulation of the incompressible Navier-Stokes equations is introduced which allows one to model boundary-layer flows induced by the motion of a deforming surface. Such a formulation may be used to model flows relevant in a wide variety of industries from polymer processing to glass manufacturing. We show that for particular sheet geometries and velocities, similarity solutions may be obtained that account for sheet thinning (or thickening) and roughness patterns observed in extrusion-type processes.

# I. INTRODUCTION

Extrusion-type processes are common and are used to produce thin sheets and fibres for a range of different materials, two primary examples being polymer extrusion and glass drawing. In polymer extrusion plastic resin is placed in a heated barrel known as an extruder where it is heated and melts. The extruder contains a rotating screw that pumps the molten polymer through a wide ($\sim$ 1-10 m), narrow ($\sim$ 1 mm) slit called a die which determines the shape of the final product. The molten polymer rapidly cools upon exiting the die where uniform cooling is required to prevent deformities. This is achieved by winding the sheet around a series of cooled rollers. These rollers can also serve to control the final dimensions of the polymer by adjusting their respective speeds. They can also be used to apply a finish to the sheet since the polymer is often soft enough on exiting the die to mirror the surface of the rollers. This finish can be aesthetic or functional. The roughness of the surface can be controlled by having different grades and patterns of roughness on the rollers. The ultimate use of the finished product depends on its gauge with thinner sheets being thermoformed for use in packaging and thicker sheets often used as a protective layer or liner for the storage and transportation of goods. In the analysis that follows we are interested in the boundary-layer flow induced by these extrusion processes. However, we will briefly discuss sheet and fibre drawing to highlight issues with many of the current studies focusing on these induced boundary-layer flows.

Extrusion flows were originally modelled experimentally by Trouton [1] who derived an empirical relationship between the velocity and thickness of a viscous fibre stretching via a tensile force. The empirical results of Trouton have been extended by numerous authors since, primarily using asymptotic expansions predicated on the small thickness-to-length ratios of the sheet (Howell [2]) or fibres (Pearson and Matovich [3]). At leading order, the streamwise velocity component $u$ is found to be independent of the radial (fibres) or wall-normal (sheets) coordinate and can be characterised by the ratio of inlet to outlet velocities known as the draw ratio $D$, such that $u = D^x$, with $x$ being the streamwise spatial coordinate. Using simple conservation of mass arguments it can be deduced that the sheet or

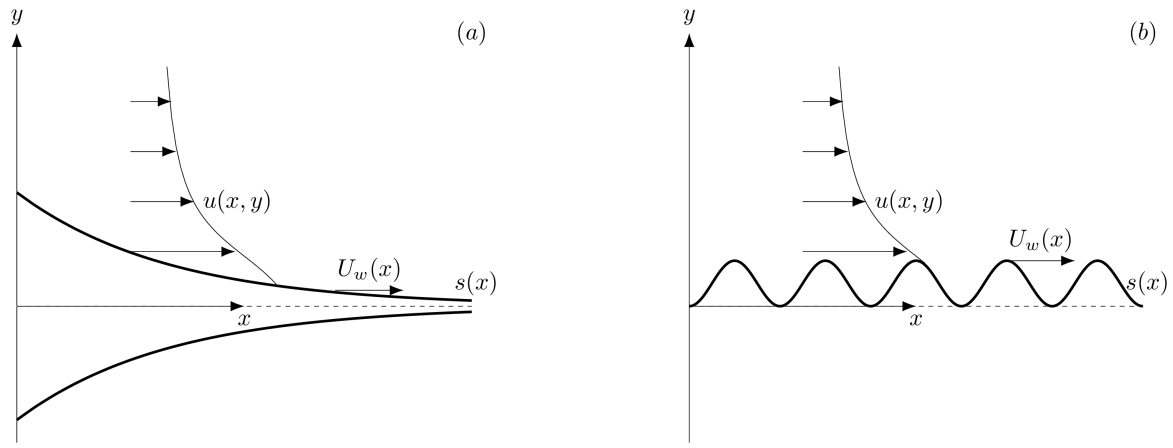


FIG. 1. Schematic diagrams of boundary-layer flows developing over (a) a stretching thinning sheet, and (b) a periodic rough surface. In both cases the profile of the surface is denoted by $s(x)$, the surface has a wall velocity denoted by $U_w(x)$, and it is this non-constant wall velocity that results in the development of a boundary-layer profile denoted by $u(x, y)$.

fibre must have a thickness $s$ defined as follows (using the notation of Fig. 1):

$$s(x) = \begin{cases} D^{-x} & \text{(sheets)}, \\ D^{-\frac{x}{2}} & \text{(fibres)}. \end{cases}$$

In spite of this analysis the majority of studies considering boundary-layer flows induced by stretching surfaces neglect the dynamics of the sheet. Instead, it is often assumed that the sheet is flat, and the stretching rate is imposed as a boundary condition, as, for example, in Crane[4], where a linear stretching rate is stipulated. While mathematically convenient, this type of formulation may have important consequences for identifying instabilities that may arise in industrial practices. For instance in Bhattacharyya and Gupta[5] a linear stability analysis on the flat, linear stretching sheet was conducted where it was concluded that the flow was linearly stable to Görtler type disturbances. However, this may not be the case in practice and such instabilities may be apparent should the thinning deformation of the sheet be taken into account.

It should be noted that this is not the first study to attempt to account for the dynamics of a sheet. In Al-Housseiny and Stone[6], the momentum equations for both viscous and elastic sheets are coupled to the momentum equations for the ambient fluid above. In doing so similarity solutions are obtained under a limiting set of constraints on the physics of both the sheet and the fluid. Similarly, Rees and Pop[7] considered boundary layer flows and

heat transfer over a wavy surface moving tangentially to itself with a constant velocity. In this article, a sinusoidal surface profile was assumed, profiles such as these have been used by others to model small-amplitude periodic surface roughness (see, for example, Yoon, Hyun, and Park[8], and Garrett *et al.*[9]). The resulting boundary layer equations were solved numerically and physical quantities such as the skin friction coefficient and rate of heat transfer were reported.

This paper follows a similar formulation to that presented by Rees and Pop[7] and bridges the gap between the analysis of flows induced by flat stretching surfaces, and the coupled sheet fluid system studied by Al-Housseiny and Stone[6]. To achieve this we effectively treat the sheet as a solid object with both its shape and velocity being prescribed in a manner that permits the existence of self-similar flow profiles. Using this formulation we also show that boundary layer flows induced by surface thickening processes, such as those observed during textile compaction, can also be modelled. Such a process is essentially the converse of the sheet-thinning processes discussed previously, whereby a material is fed into a compactor at a greater speed than it is extracted. These types of processes exploit the fact that fibrous materials exhibit viscoelastic behaviour[10]. Here this is manifested as an increase in stress within the fibre after a compaction-relaxation cycle which prevents the fibre from recovering to its initial volume. There is a wealth of literature attempting to explain this phenomenon and an overview of different modelling approaches is provided in Kelly[11]. Furthermore, our formulation can also be used to model boundary-layer flows generated by the extrusion of small-amplitude rough surfaces where here we consider a periodic roughness profile similar to that discussed by Yoon, Hyun, and Park[8].

The remainder of the paper is structured as follows. In Sec. II the boundary-layer equations for flows induced by deforming surfaces are derived. This is achieved by first performing a coordinate system transformation to "flatten" the sheet before applying the usual large Reynolds number boundary-layer scaling. In Sec. III we look at particular combinations of surface shapes and wall velocities in order to model sheet thinning or thickening processes as well as boundary-layer flows generated by the extrusion of rough surfaces. We show that under certain limiting assumptions, analytical boundary-layer solutions may be derived. As one would expect, these results are dependent on the physics of the system being considered, those being the exact profile of the deforming surface and the wall velocity of said surface. The analysis that we present is generalised. However, all the solutions can be tailored to

model flows that are observed in practice given sufficient knowledge of the above physical constraints. To conclude, in Sec. III, we present a numerical validation of our analytical thinning sheet solutions using a finite element approach. Lastly, in Sec. IV, we present a discussion regarding both our findings and the potential for future work.

## II. PROBLEM FORMULATION

Consider the steady flow of an incompressible, Newtonian fluid over an impermeable, semi-infinite plate. The streamwise coordinate is $x^*$, and the wall-normal coordinate is $y^*$ (asterisks denotes dimensional quantities). This flow is governed by the continuity and Navier-Stokes momentum equations,

$$\boldsymbol{\nabla}^* \cdot \mathbf{u}^* = 0, \tag{1a}$$

$$\rho^*(\mathbf{u}^* \cdot \boldsymbol{\nabla}^*)\mathbf{u}^* = -\boldsymbol{\nabla}^* p^* + \mu^* \Delta^* \mathbf{u}^*. \tag{1b}$$

The fluid density is $\rho^*$, the dynamic viscosity is $\mu^*$, the pressure is $p^*$, and the velocity field is $\mathbf{u}^* = (u^*, v^*)$, where $u^*$, and $v^*$ are the velocity components in the streamwise and wall-normal directions, respectively. In what follows we consider boundary-layer flows over non-flat surfaces for $x^* \in [0, \infty)$, as such, it proves useful to introduce a change in coordinate system with $\xi^* = x^*$, and $\eta^* = y^* - s^*$, where $s^*(x^*)$, is the function that describes the variation of the surface height of the plate. The transformed governing equations are then

$$\frac{\partial u^*}{\partial \xi^*} + \frac{\partial \tilde{v}^*}{\partial \eta^*} = 0, \tag{2a}$$

$$u^* \frac{\partial u^*}{\partial \xi^*} + \tilde{v}^* \frac{\partial u^*}{\partial \eta^*} = -\frac{1}{\rho^*}\frac{\partial p^*}{\partial \xi^*} + \nu^* \mathcal{L}_1^* u^* + \frac{1}{\rho^*}\frac{\mathrm{d}s^*}{\mathrm{d}\xi^*}\frac{\partial p^*}{\partial \eta^*}, \tag{2b}$$

$$u^* \frac{\partial \tilde{v}^*}{\partial \xi^*} + \tilde{v}^* \frac{\partial \tilde{v}^*}{\partial \eta^*} + \frac{\mathrm{d}^2 s^*}{\mathrm{d}\xi^{*2}} u^{*2} = -\frac{\sigma^{*2}}{\rho^*}\frac{\partial p^*}{\partial \eta^*} + \nu^* \mathcal{L}_1^* \tilde{v}^* + \frac{1}{\rho^*}\frac{\mathrm{d}s^*}{\mathrm{d}\xi^*}\frac{\partial p^*}{\partial \xi^*} + \nu^* \mathcal{L}_2^* u^*, \tag{2c}$$

where $\nu^* = \mu^*/\rho^*$ is the kinematic viscosity, and the differential operators are

$$\mathcal{L}_1^* = \frac{\partial^2}{\partial \xi^{*2}} - \frac{\mathrm{d}^2 s^*}{\mathrm{d}\xi^{*2}}\frac{\partial}{\partial \eta^*} - 2\frac{\mathrm{d}s^*}{\mathrm{d}\xi^*}\frac{\partial^2}{\partial \xi^* \partial \eta^*} + \sigma^{*2}\frac{\partial^2}{\partial \eta^{*2}}, \tag{2d}$$

$$\mathcal{L}_2^* = 2\frac{\mathrm{d}^2 s^*}{\mathrm{d}\xi^{*2}}\left(\frac{\partial}{\partial \xi^*} - \frac{\mathrm{d}s^*}{\mathrm{d}\xi^*}\frac{\partial}{\partial \eta^*}\right) + \frac{\mathrm{d}^3 s^*}{\mathrm{d}\xi^{*3}}. \tag{2e}$$

In the $\xi$-$\eta$ coordinate system the wall-normal velocity is defined as

$$\tilde{v}^* = v^* - \frac{\mathrm{d}s^*}{\mathrm{d}\xi^*}u^*, \tag{2f}$$

and the function $\sigma^*$ is expressed as

$$\sigma^* = \sqrt{1 + \left(\frac{\mathrm{d}s^*}{\mathrm{d}\xi^*}\right)^2}. \tag{2g}$$

We note that function $\sigma^*$ is related to the curvature of the surface $\kappa^*$ as follows:

$$\kappa^*(\xi^*) = \frac{1}{\sigma^{*2}} \frac{\mathrm{d}\sigma^*}{\mathrm{d}\xi^*} \left(\frac{\mathrm{d}s^*}{\mathrm{d}\xi^*}\right)^{-1}.$$

System (2) is solved subject to the wall conditions $\mathbf{u}^* \cdot \hat{\mathbf{t}} = U_w^*(\xi^*)$, and $\mathbf{u}^* \cdot \hat{\mathbf{n}} = 0$, where $U_w^* \geq 0$, is the dimensional wall velocity. In this transformed coordinate system, in the absence of any oncoming flow, the relevant boundary conditions for this problem are then

$$u^*(\eta^* = 0) = U_w^*(\xi^*)/\sigma^*(\xi^*), \quad \tilde{v}^*(\eta^* = 0) = 0, \quad u^*(\eta^* \to \infty) \to 0. \tag{3}$$

These conditions ensure that there is always no flow normal to the surface (no penetration), and that the surface moves tangentially to itself with velocity $U_w^*$. We consider the development of a boundary-layer due to the non-constant wall velocity $[U_w^* = U_w^*(\xi^*)]$ of the plate. For example, the case when $U_w^* = C^*\xi^*$, corresponds to linear stretching of the surface with the constant $C^*$ having units $\mathrm{s}^{-1}$. This problem, in the non-deformed frame of reference, has been well studied and was first considered by Crane [4]. We will show that it is not possible to determine self-similar solutions when the plate is subject to a constant wall velocity and is not flat.

The problem is non-dimensionalised as follows:

$$(\xi, Y, s) = \frac{(\xi^*, \eta^*, s^*)}{L^*}, \quad (u, \tilde{v}, U_w) = \frac{(u^*, \tilde{v}^*, U_w^*)}{U^*}, \quad p = \frac{p^*}{\rho^* U^{*2}},$$

where $U^*$, and $L^*$, are reference velocity and length scales, respectively. In order to then arrive at the relevant boundary-layer equations the following scalings are introduced

$\eta = \mathrm{Re}^{1/2}\, Y$, and $v = \mathrm{Re}^{1/2}\, \tilde{v}$, where $\mathrm{Re} = U^* L^*/\nu^*$. Therefore system (2) reduces to

$$\frac{\partial u}{\partial \xi} + \frac{\partial v}{\partial \eta} = 0, \tag{4a}$$

$$\begin{aligned} u\frac{\partial u}{\partial \xi} + v\frac{\partial u}{\partial \eta} = {} & s'_\xi\, \mathrm{Re}^{1/2}\, \frac{\partial p}{\partial \eta} - \frac{\partial p}{\partial \xi} + \sigma^2 \frac{\partial^2 u}{\partial \eta^2} \\ & - \frac{1}{\mathrm{Re}^{1/2}} \left( s''_{\xi\xi} \frac{\partial u}{\partial \eta} + 2 s'_\xi \frac{\partial^2 u}{\partial \xi \partial \eta} \right) + \frac{1}{\mathrm{Re}} \frac{\partial^2 u}{\partial \xi^2}, \end{aligned} \tag{4b}$$

$$\begin{aligned} \frac{1}{\mathrm{Re}} \left( u\frac{\partial v}{\partial \xi} + v\frac{\partial v}{\partial \eta} \right) + \frac{s''_{\xi\xi} u^2}{\mathrm{Re}^{1/2}} = {} & \frac{s'_\xi}{\mathrm{Re}^{1/2}} \frac{\partial p}{\partial \xi} - \sigma^2 \frac{\partial p}{\partial \eta} + \frac{\sigma^2}{\mathrm{Re}} \frac{\partial^2 v}{\partial \eta^2} \\ & - \frac{1}{\mathrm{Re}^{3/2}} \left( s''_{\xi\xi} \frac{\partial v}{\partial \eta} + 2 s'_\xi \frac{\partial^2 v}{\partial \xi \partial \eta} \right) + \frac{1}{\mathrm{Re}^2} \frac{\partial^2 v}{\partial \xi^2} \\ & + \frac{1}{\mathrm{Re}} \left[ 2 s''_{\xi\xi} \left( \frac{1}{\mathrm{Re}^{1/2}} \frac{\partial u}{\partial \xi} - s'_\xi \frac{\partial u}{\partial \eta} \right) + \frac{s'''_{\xi\xi\xi} u}{\mathrm{Re}^{1/2}} \right], \end{aligned} \tag{4c}$$

where the primes with associated subscripts denote differentiation with respect to the subscript variable and $\sigma^2 = 1 + (s'_\xi)^2$. In order to determine the correct leading order balance the following expansions are introduced:

$$\begin{aligned} u(\xi, \eta) = {} & u_0(\xi, \eta) + \mathrm{Re}^{-1/2}\, u_1(\xi, \eta) + \cdots, \\ v(\xi, \eta) = {} & v_0(\xi, \eta) + \mathrm{Re}^{-1/2}\, v_1(\xi, \eta) + \cdots, \\ p(\xi, \eta) = {} & p_0(\xi) + \mathrm{Re}^{-1/2}\, p_1(\xi, \eta) + \cdots, \end{aligned}$$

where, to leading order, the pressure is a function of $\xi$ only [this can be directly inferred from (4c)]. Thus, the leading order boundary-layer equations for these classes of problems are as follows

$$\frac{\partial u_0}{\partial \xi} + \frac{\partial v_0}{\partial \eta} = 0, \tag{5a}$$

$$u_0 \frac{\partial u_0}{\partial \xi} + v_0 \frac{\partial u_0}{\partial \eta} + \sigma^{-1} \sigma'_\xi u_0^2 = -\sigma^{-2} (p_0)'_\xi + \sigma^2 \frac{\partial^2 u_0}{\partial \eta^2}. \tag{5b}$$

This system is the Newtonian equivalent of the non-Newtonian equations derived, for example, by Pop and Nakamura [12]. In the case when the plate is flat, i.e., $s$ is constant, the above reduces to the familiar 2D boundary-layer equations. Outside the boundary layer the flow must match with the far-field stationary flow, $U_\infty = 0$. By considering the behaviour of equation (5b) at a large distance from the surface of the plate the pressure, to leading

order, is determined to be constant. Thus,

$$\frac{\partial u_0}{\partial \xi} + \frac{\partial v_0}{\partial \eta} = 0, \tag{6a}$$

$$u_0 \frac{\partial u_0}{\partial \xi} + v_0 \frac{\partial u_0}{\partial \eta} + \sigma^{-1}\sigma'_\xi u_0^2 = \sigma^2 \frac{\partial^2 u_0}{\partial \eta^2}. \tag{6b}$$

The above system is then closed subject to the following conditions:

$$u_0(\eta = 0) = U_w(\xi)/\sigma(\xi), \quad v_0(\eta = 0) = 0, \quad u_0(\eta \to \infty) \to 0. \tag{6c}$$

This system of boundary-layer equations is general in the sense that one is not restricted by any of the dynamics of the deforming surface. In what follows we seek to extend previous analyses and wish to determine self-similar solutions of (6) subject to (6c) without *a priori* knowledge of either the deforming surface profile or the wall velocity.

## III. SELF-SIMILAR FLOWS

Assuming that (6) admits self-similar solutions we introduce the similarity coordinate

$$\zeta = \frac{\eta}{g}\sqrt{\frac{U_w}{\xi\sigma}},$$

and the streamfunction $\psi = g\sqrt{U_w \xi/\sigma} f(\zeta)$, where $g$ is a yet to be determined function of $\xi$. These expressions for $\zeta$ and $\psi$ are informed by standard boundary-layer scalings[13] and also the need to ensure that $u_0$ is proportional to both the wall velocity and the inverse of the function $\sigma$. We note that in the case when the wall velocity is constant and the surface is flat the unknown quantity $g$ can be removed from these expressions and the analysis follows identically that of Tsou, Sparrow, and Kurtz[13].

Given the preceding definitions it follows immediately that

$$\begin{aligned} u_0 =& \frac{\partial \psi}{\partial \eta} = (U_w/\sigma) f'_\zeta, \\ v_0 =& -\frac{\partial \psi}{\partial \xi} = g\sqrt{U_w \xi/\sigma}(\zeta f'_\zeta X_- - f X_+), \end{aligned}$$

where

$$X_\pm = \frac{g'_\xi}{g} + \frac{1}{2\xi} \pm \frac{1}{2}\left[\frac{(U_w)'_\xi}{U_w} - \frac{\sigma'_\xi}{\sigma}\right].$$

Therefore (6b) reduces to

$$\xi g^2[-X_+ f f''_{\zeta\zeta} + U_w^{-1}(U_w)'_\xi (f'_\zeta)^2] = \sigma^2 f'''_{\zeta\zeta\zeta}.$$

In order to be able to determine similarity solutions it must then be the case that

$$\xi g^2 X_+ = c_1 \sigma^2, \tag{7a}$$

$$\xi g^2 U_w^{-1} (U_w)'_\xi = c_2 \sigma^2, \tag{7b}$$

where $c_1$ and $c_2$ are arbitrary constants that ensure self-similarity. The instances when one of these constants is set equal to zero, with the other being non-zero, are considered in Appendix A. Rearranging (7b) gives $g^2 = c_2 \sigma^2 U_w [\xi (U_w)'_\xi]^{-1}$. Substituting this form for $g^2$ into (7a) one then removes the unknown function $g$ from the problem and arrives at the following second order ODE

$$U_w \frac{\mathrm{d}^2 U_w}{\mathrm{d}\xi^2} + \gamma \left( \frac{\mathrm{d}U_w}{\mathrm{d}\xi} \right)^2 - \mathcal{S} U_w \frac{\mathrm{d}U_w}{\mathrm{d}\xi} = 0, \tag{8}$$

where $\mathcal{S} = [\ln(\sigma)]'_\xi$, and $\gamma = 2(c_1 - c_2)/c_2$. We note that the above equation is identically satisfied when $U_w =$ constant. However, (7b) would then imply that $c_2 = 0$. This special case is considered in Appendix A. Given the form of (8) there are two distinct cases to consider, when $\gamma = -1$, and when $\gamma \neq -1$. In the first case, the substitution $R = [\ln(U_w)]'_\xi$, reduces the order of (8) such that

$$\frac{\mathrm{d}R}{\mathrm{d}\xi} - \mathcal{S} R = 0.$$

Therefore $R = K\sigma$, where $K$ is a constant of integration, and it follows immediately that

$$(U_w)'_\xi = K U_w \sigma. \tag{9}$$

In the second case, when $\gamma \neq -1$, the substitution $R = (1+\gamma) U_w^{1+\gamma} [\ln(U_w)]'_\xi$, leads to the same first order ODE. Therefore, in these cases

$$(U_w)'_\xi = \frac{K\sigma}{(1+\gamma) U_w^\gamma}. \tag{10}$$

This ODE can be rewritten as such

$$W'_\xi = K\sigma, \tag{11}$$

where $W = U_w^{1+\gamma}$. Thus, irrespective of the value of $\gamma$, in order to be able to determine similarity solutions, one may choose either to specify the wall velocity, $U_w$, and calculate the variation of the height of the plate, $s$, or specify $s$ and determine the required form for

$U_w$. With $s$ fixed the determination of $U_w$ transpires to be a relatively simple procedure. Integrating (9) and (11) respectively we have that

$$U_w = \begin{cases} C\,\mathrm{e}^{K\mathcal{I}} & \text{when} \quad \gamma = -1, \\ (C + K\mathcal{I})^{\frac{1}{1+\gamma}} & \text{when} \quad \gamma \neq -1, \end{cases} \tag{12}$$

where $C$ is a constant of integration and $\mathcal{I}$ is simply the arc length of the surface,

$$\mathcal{I} = \int \sigma(\xi)\,\mathrm{d}\xi = \int \sqrt{1 + (s'_\xi)^2}\,\mathrm{d}\xi. \tag{13}$$

Therefore, for any fixed $s$ it is possible to determine $U_w$, for any value of $\gamma$, simply by integrating the function $\sigma$. It is clear from the above analysis that the value of the constant $\gamma$ dictates the form of the wall velocity. In cases when $\gamma \geq -1$ the deforming surface will be accelerating whilst the inverse is true when $\gamma < -1$. As an example, a deforming surface that is being thinned as it is being stretched would, by mass conservation, have to be accelerating.

Now, by writing $\hat{f}(Z) = \sqrt{c_1} f(\zeta)$, where $Z = \sqrt{c_1}\zeta$, then $\hat{f}'_Z = f'_\zeta$, and the ODE that governs the base flow is then given by

$$\hat{f}'''_{ZZZ} + \hat{f}\hat{f}''_{ZZ} - \left(\frac{2}{2+\gamma}\right)(\hat{f}'_Z)^2 = 0. \tag{14a}$$

The case when $\gamma = -2$ is considered separately in Appendix A. The preceding ODE must be solved subject to

$$\hat{f}(Z=0) = 0, \quad \hat{f}'_Z(Z=0) = 1, \quad \hat{f}'_Z(Z \to \infty) \to 0. \tag{14b}$$

It is worth noting that (14) admits exact analytical solutions for two specific $\gamma$ values. In the case when $\gamma = 0$, then $\hat{f} = 1 - \mathrm{e}^{-Z}$, whilst when $\gamma = -4$, then $\hat{f} = \sqrt{2}\tanh(Z/\sqrt{2})$. A derivation of these solutions using a similar approach to those employed in Ackroyd [14] and Sachdev, Bujurke, and Pai [15] may be found in Appendix B. In what follows we will highlight three specific case studies that make use of these exact solutions and a numerical solution of (14), although we note that the choice of the value of the constant $\gamma$ would, in practice, be informed by experimental conditions.

In order to verify the previous analysis we consider Crane's problem. Crane's problem corresponds to the linear stretching of a flat plate, as such, $s$ is a constant and (11) reduces simply to $(U_w)'_\xi = K$. Thus when $K = 1$, and stipulating that $U_w(\xi = 0) = {}_0U_w = 0$, we recover the expected linear stretching result; $U_w = \xi$. In order to be able to visualise

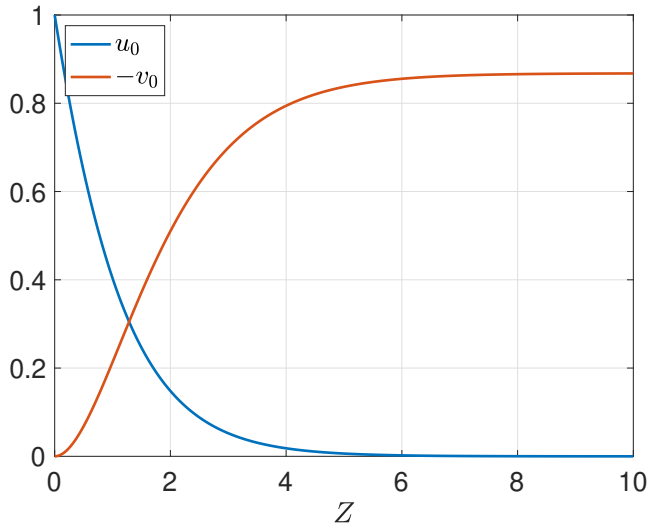


FIG. 2. Plots of the streamwise and wall-normal velocity components for the case when $\gamma = 2$ and $U_w = \sqrt{{}_0U_w^2 + 2\xi/3} = \sigma$. In this case both $u_0$ and $v_0$ are independent of $\xi$. Given that no exact analytical solution for $\hat{f}$ exists in the case when $\gamma = 2$, a shooting method that makes use of a fourth-order Runge-Kutta integrator, twinned with a secant root finding scheme, was employed to solve (14). As part of this solution process we determine that $\hat{f}''_{ZZ}(Z = 0) \approx 0.8300$, and that $\hat{f}(Z \to \infty) = \hat{f}_\infty \approx 1.0625$. In the limit as $Z \to \infty$, then $v_0 \to -\sqrt{2/3}\hat{f}_\infty$.

the solutions for both $u_0$ and $v_0$ one needs to recall the unknown function $g$ such that the similarity coordinate $Z$, and streamfunction $\psi$, can be written in terms of known functions. Irrespective of the value of $\gamma$ we have that

$$g = \sqrt{\frac{2c_1\alpha\sigma U_w^{1+\gamma}}{K\xi}},$$

where

$$\alpha = \begin{cases} 1 & \text{when} \quad \gamma = -1, \\ (1+\gamma)(2+\gamma)^{-1} & \text{when} \quad \gamma \neq -1. \end{cases}$$

In order to ensure that $g$ is solely real then, given that $c_1 > 0$, the constant $K$ would have to be negative in the cases when $-2 < \gamma < -1$. Given the form of (12), with $\gamma$ in this range and $K$ being less than zero, one would then determine complex solutions for the wall velocity. Therefore, physical solutions are derived only in the cases when $\gamma < -2$, and $\gamma \geq -1$. For convenience we now fix $K$ equal to unity but note that the following analysis holds for any $K > 0$. Having done so we determine that $\psi = \varsigma U_w \hat{f}(Z)$, where $Z = \eta/(\varsigma\sigma)$,

and $\varsigma = \sqrt{2\alpha U_w^{\gamma}}$. Thus

$$u_0 = \frac{\partial \psi}{\partial \eta} = \left(\frac{U_w}{\sigma}\right)\hat{f}'_Z,$$
$$v_0 = -\frac{\partial \psi}{\partial \xi} = \frac{\varsigma}{2}\left\{\left[\frac{2U_w\sigma'_\xi}{\sigma} + \gamma(U_w)'_\xi\right]Z\hat{f}'_Z - (2+\gamma)(U_w)'_\xi\hat{f}\right\}.$$

There is clearly a special case to consider when $U_w$ is directly proportional to $\sigma$. In this case then both $u_0$, and $v_0/\varsigma$ are functions of $Z$ only. In addition to this, setting $\gamma = 2$, and fixing $U_w = \sigma$ ensures that $u_0 = \hat{f}'_Z$, and $v_0 = \sqrt{2/3}(Z\hat{f}'_Z - \hat{f})$, i.e., the wall-normal velocity is then identically independent of the streamwise coordinate $\xi$ (see Fig. 2). Recalling (11) it must then transpire that $(U_w)'_\xi = 1/(3U_w)$. Thus, imposing the condition that the initial wall velocity is equal to ${}_0U_w$, then $U_w = \sqrt{{}_0U_w^2 + 2\xi/3} = \sigma$. Given this form for $\sigma$, and stipulating that $s(\xi = 0) = s_0$, it must therefore be the case that $s(\xi) = s_0 - ({}_0U_w^2 - 1)^{3/2} + ({}_0U_w^2 - 1 + 2\xi/3)^{3/2}$. Practically, it is perhaps unphysical to consider a case whereby the variation of the surface height of the plate is increasing in such a manner. However, given the preceding analysis we are now in a position to consider a number of cases that closely resemble physical boundary layer flows.

### A. Surface Thinning

In order to capture the realistic thinning nature of a sheet that is being extruded from a cast die we fix the dimensional surface height of the plate such that

$$s^*(\xi^*) = a_1^*\,\mathrm{e}^{-(\xi^*/a_2^*)}.$$

Given this form for $s^*$, we define our non-dimensionlaising length scale $L^*$ as the inlet sheet height $a_1^*$, so that $s(\xi) = \mathrm{e}^{-a\xi}$, where $a = a_1^*/a_2^*$, and $\sigma = \sqrt{1 + a^2\mathrm{e}^{-2a\xi}}$. Therefore we have that

$$\mathcal{I} = \frac{\operatorname{arcsinh}(a^{-1}\mathrm{e}^{a\xi}) - \sigma}{a}.$$

Thus an analytical expression for $U_w$ can be determined directly from (12). In practice one would choose the free constants $(a, \gamma)$ such that the wall velocity profile matched closely with physical observations. In the absence of experimental data we are free to choose mathematically convenient values for these constants. If we set $a = \gamma + 1 = 1$, and stipulate that $U_w(\xi = 0) = {}_0U_w = 0$, then it follows that

$$U_w = \xi + \ln\left(\frac{1+\sigma}{1+\sigma_0}\right) + \sigma_0 - \sigma,$$

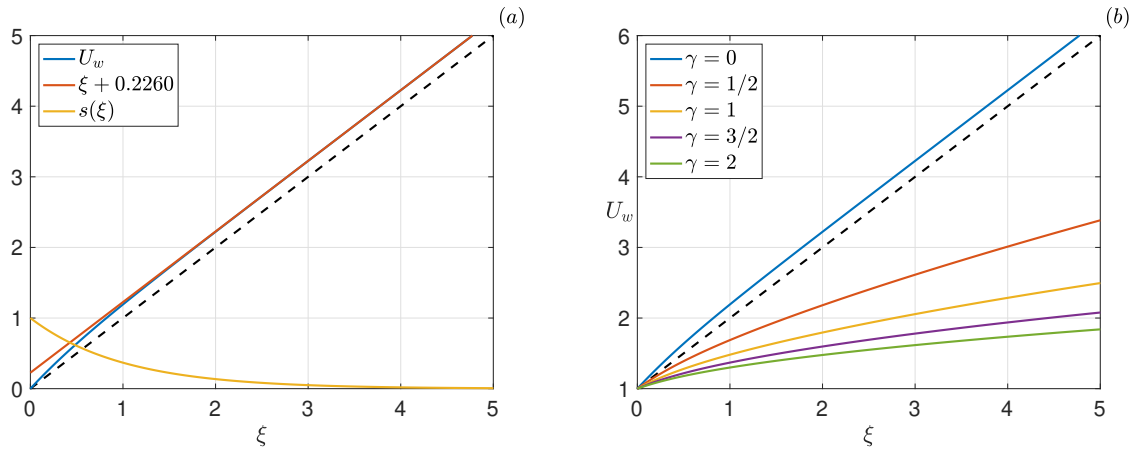


FIG. 3. In (a) the wall velocity $U_w$, the approximate wall velocity $U_w^{\text{approx}} = \xi + 0.2260$, and the exponentially thinning sheet profile: $s(\xi) = \mathrm{e}^{-\xi}$, are plotted against $\xi$. In (b) the wall velocity, given an identical thinning sheet profile, is plotted for a range of $\gamma$ values. In both plots the dashed black line corresponds to the wall velocity result for a sheet undergoing linear stretching.

where, in this case, $\sigma_0 = \sigma(\xi = 0) = \sqrt{2}$. This expression for $U_w$ is reasonably close to the result owing from Crane's linear stretching problem ($U_w = \xi$). Aside from the region close to $\xi = 0$, we find that $U_w$ can be approximated in the following fashion

$$U_w^{\text{approx}} = \xi + \ln\left(\frac{2}{1+\sigma_0}\right) + \sigma_0 - 1 \approx \xi + 0.2260.$$

This result, presented graphically in Fig. 3, is perhaps not surprising given that the sheet is thinning exponentially. As such, we would expect to recover a result for the wall velocity similar to that of Crane[4] in all regions where the plate is locally flat. However, we note that the analysis presented here is general enough that one could consider a plethora of different thinning sheet profiles dependent on the value of the constant $a$, or the rate of sheet acceleration depending on the value of $\gamma$.

The results presented in Fig. 4 show the discrepancy between the solutions obtained under the assumption of a flat stretching sheet when compared to those obtained under the correct assumption that the sheet will thin as it is accelerated and stretched. We observe that the streamwise velocity component is always under-predicted by Crane's model. Furthermore, near to the point where the sheet is being extruded, when $\xi = 0$, we observe that the gradient of the wall-normal velocity component is significantly shallower under the assumption that the surface does not deform as it stretches. The disparity of these results at the surface

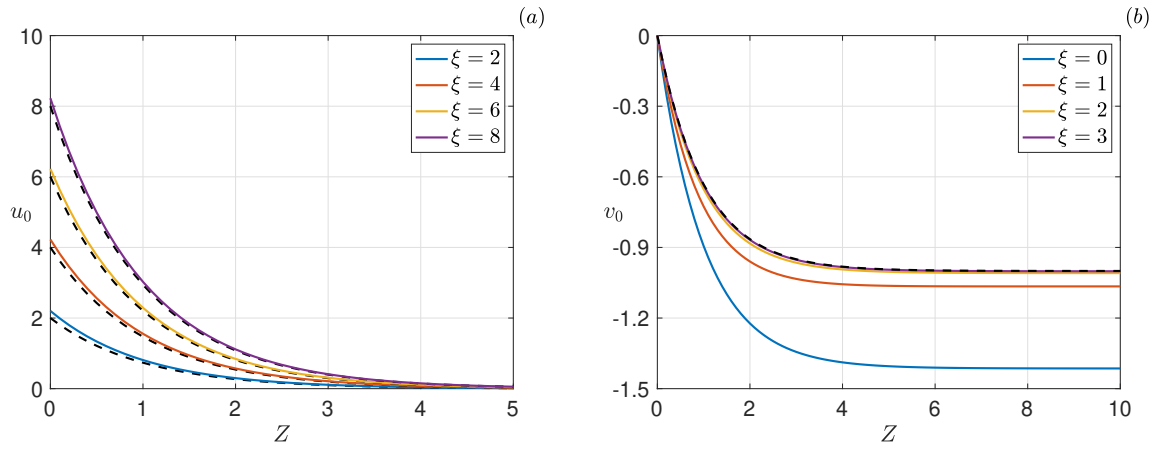


FIG. 4. Plots of the streamwise (a) and wall-normal (b) velocity components for a range of $\xi$ values. In this case the sheet is thinning exponentially: $s(\xi) = \mathrm{e}^{-\xi}$. Crane's flat plate solutions are given by the dashed black curves.

of the sheet leads to a significant under-prediction of the magnitude of the flow that, via mass conservation, is directed towards the stretching surface. We note that these effects are exacerbated when the constant $a$ decreases in value. Irrespective of the value of this constant, at a sufficiently large enough distance downstream, the wall-normal velocity profile will, however, always tend towards Crane's solution since the plate is locally flat as $\xi \to \infty$. Similar qualitative results are obtained if one assumes that the sheet deforms in either a polynomial or a logarithmic manner.

## B. Surface Thickening

Theoretical studies of textile compaction processes[11] have sought to model the stress within a fibre over a compaction relaxation-cycle. Here our aim is to propose a shape which captures the resulting reduction in volume fraction and hence determine a sheet velocity profile which facilitates a self-similar boundary layer solution for the ambient fluid. While this approach represents a simplification of the underlying physics governing such processes, it is warranted by the observed tendency of compaction-induced defects to manifest in textile manufacturing. These defects are commonly ascribed to micro-mechanical phenomena arising from the closure of interstitial gaps between individual fibres in a composite sheet, as described in Thompson *et al.*[16]. However, an examination of the stability characteristics

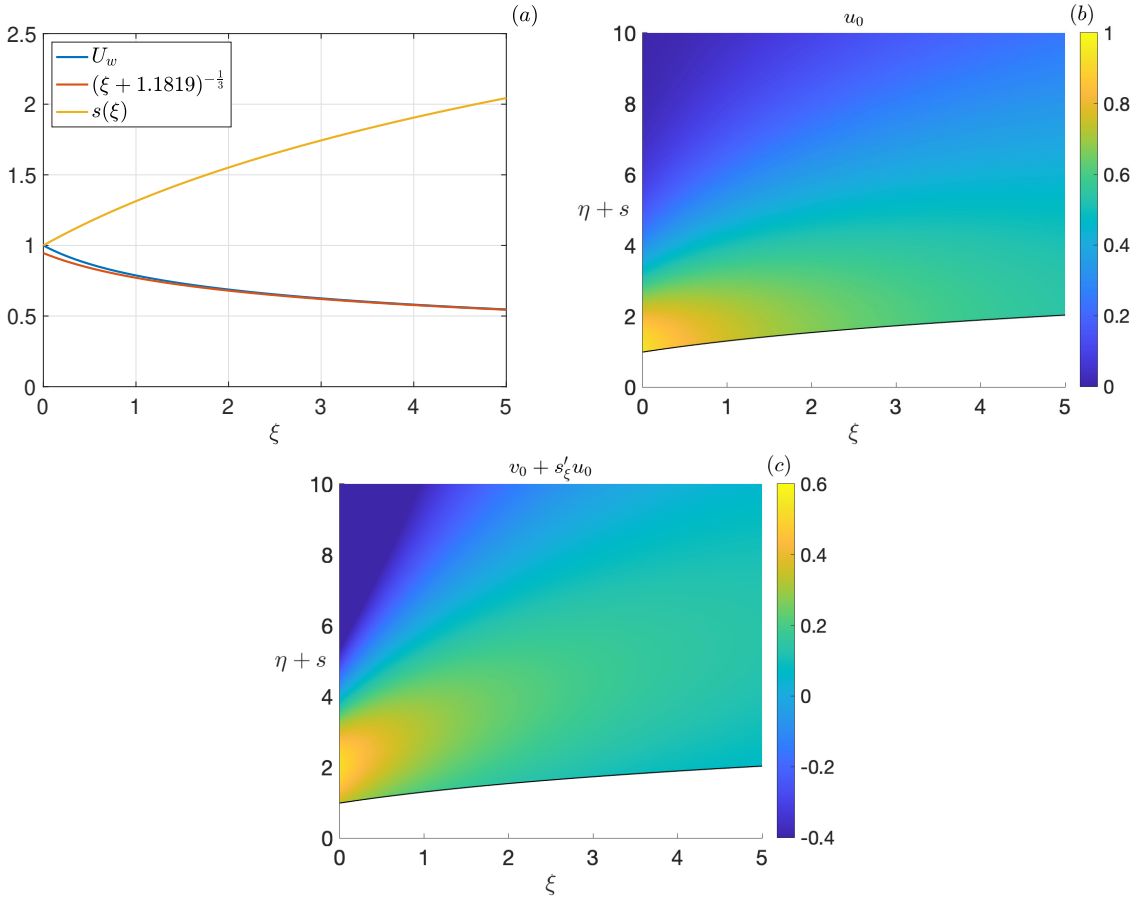


FIG. 5. In (a) the wall velocity $U_w$, the approximate wall velocity $U_w^{\text{approx}} = (\xi + 1.1819)^{-\frac{1}{3}}$, and the logarithmically thickening sheet profile, $s(\xi) = \ln(\mathrm{e} + \xi)$, are plotted against $\xi$. In (b) and (c), respectively, solutions for the streamwise velocity $u_0$ and wall-normal velocity $v_0 + s'_\xi u_0$ are mapped back to the unscaled boundary-layer coordinate system $(\xi, \eta + s)$. The solid black line indicates the surface of the thickening decelerating sheet.

of the induced boundary layer might provide insights into the potential mitigation of such defects.

If we consider a deforming surface with a profile defined as such, $s^*(\xi^*) = b_1^* \ln(\mathrm{e} + \xi^*/b_2^*)$, where e is the exponential constant chosen such that $s^*(\xi^* = 0) = b_1^*$, then such a profile can be used to model a thickening, decelerating surface such as those observed in compaction processes. We again set $L^* = b_1^*$, the initial sheet thickness, so that $s(\xi) = \ln(\mathrm{e} + b\xi)$ with $b = b_1^*/b_2^*$. Irrespective of the value of $b$, in order to determine similarity solutions we first compute

$$\mathcal{I} = \frac{(\mathrm{e} + b\xi)}{b}\sigma - \operatorname{arcsinh}(s'_\xi).$$

Here we choose the convenient parameter value $b = 1$, such that via (12) we have, for $\gamma \neq -1$, that

$$U_w = [C + (\mathrm{e} + \xi)\sigma - \operatorname{arcsinh}(s'_\xi)]^{\frac{1}{1+\gamma}}.$$

Setting $\gamma = -4$, to ensure that the sheet is decelerating, and fixing the value of $C$ such that ${}_0U_w = 1$, we have that

$$U_w = \left[\xi\sigma + \ln\left(\frac{1 + \mathrm{e}\,\sigma_0}{s'_\xi + \sigma}\right) + \mathrm{e}\,(\sigma - \sigma_0)\right]^{-\frac{1}{3}},$$

where, in this case, $\sigma_0 = \sigma(\xi = 0) = \sqrt{1 + \mathrm{e}^{-2}}$. At first inspection, this expression for the wall velocity appears to be reasonably intricate. However, away from the region of the sheet inlet, this expression can be well approximated as follows

$$U_w^{\text{approx}} = [\xi + \ln(1 + \mathrm{e}\,\sigma_0) + \mathrm{e}\,(1 - \sigma_0)]^{-\frac{1}{3}} \approx (\xi + 1.1819)^{-\frac{1}{3}}.$$

Given that, in the case when $\gamma = -4$, we have an analytical solution for (14), with $U_w$ calculated as above, we are then able to use our stream function definitions for $u_0$ and $v_0$ to visualise the flow in terms of the unscaled boundary-layer coordinate, $\varsigma\sigma Z + s = \eta + s$. These results are depicted in Fig. 5 where we observe that both the streamwise and wall-normal fluid velocities are at a maximum in the vicinity of the inlet ($\xi = 0$). As one would expect, as both the curvature of the sheet and the velocity of the sheet decrease, the magnitude of these velocities also decreases.

### C. Surface Roughness

Given our generic problem formulation we are also able to consider the development of boundary layer flows over small-amplitude rough surfaces. Taking inspiration from Yoon, Hyun, and Park [8], if we assume a surface roughness profile of the form

$$s^*(\xi^*) = A^*[1 - \cos(2\pi\xi^*/\lambda^*)],$$

then $s_0 = 0$. Here $A^*$ and $\lambda^*$ are the amplitude and wavelength of the surface roughness, respectively. Consistent with the analysis of Yoon, Hyun, and Park [8] we set $L^* = \lambda^*$ so that $s(\xi) = \varepsilon[1 - \cos(2\pi\xi)]$, where $\varepsilon = A^*/\lambda^*$.

In what follows we will consider the case when $\varepsilon \ll 1$. Although the analysis itself is not necessarily restricted by the value of $\varepsilon$, we find that our solutions are fully parameterised

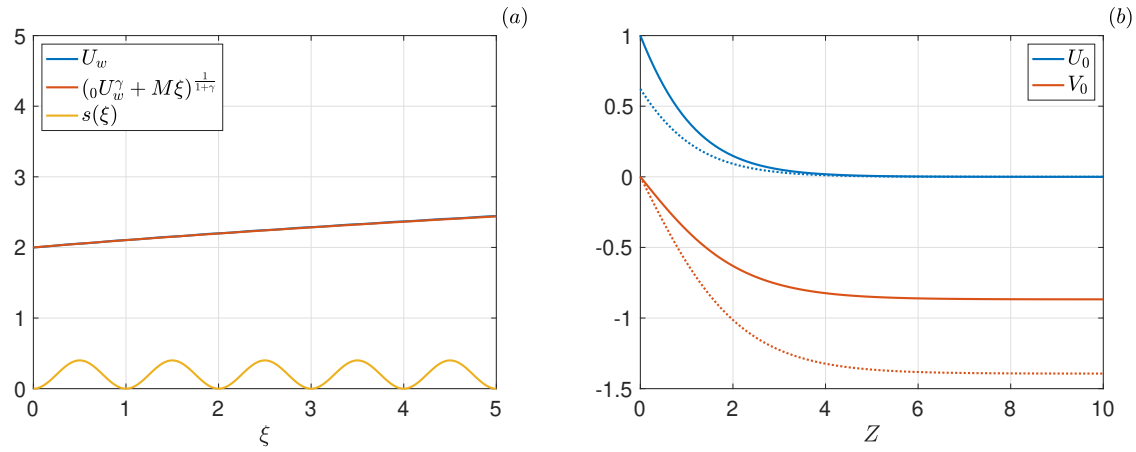


FIG. 6. In (a) the wall velocity $U_w$, the approximate wall velocity $U_w^{\text{approx}} = ({}_0U_w^\gamma + M\xi)^{\frac{1}{1+\gamma}}$, and the small-amplitude rough profile: $s(\xi) = \varepsilon[1 - \cos(2\pi\xi)]$, are plotted against $\xi$. In (b) the cyclical velocities $U_0$ and $V_0$ are plotted against the boundary-layer coordinate $Z$. The solid curves correspond to the solutions at $2\xi = (n-1)$, the dotted curves are the solutions at $2\xi = (n - \frac{1}{2})$, for $n = 1, 2, 3, \ldots$. In both instances $\varepsilon = 1/5$, ${}_0U_w = 2$, and $\gamma = 2$.

by the constant $\varepsilon$, i.e., our boundary-layer flow profiles are invariant upon changing $A^*$ and $\lambda^*$, given that their ratio, $\varepsilon$, is itself fixed.

Given the sinusoidal form for $s(\xi)$ it follows that $\sigma = [1 + (2\varepsilon\pi)^2 \sin^2(2\pi\xi)]^{1/2}$. Thus

$$\mathcal{I} = \frac{1}{2\pi} E\left(2\pi\xi \,\middle|\, -(2\pi\varepsilon)^2\right),$$

where $E(\phi \,|\, k)$ is the incomplete elliptic integral of the second kind (see Abramowitz and Stegun [17]). In the cases when $\varepsilon \ll 1$, this integral can be very well approximated in the following manner:

$$\mathcal{I} \approx \frac{\max(\sigma) + \min(\sigma)}{2}\xi = \frac{\sqrt{1 + (2\varepsilon\pi)^2} + 1}{2}\xi = M\xi,$$

where $M$ is the mid-range of the function $\sigma$. In fact, for flows generated by small-amplitude rough surfaces, the difference between the exact form of $U_w$ determined via (12), and the form based on the approximate value of $\mathcal{I}$ is graphically indistinguishable. This fact is evidenced in Fig. 6 for the case when $\varepsilon = 1/5$, ${}_0U_w = 2$, and $\gamma = 2$. Having set $\gamma = 2$ we observe that the sheet undergoes only very moderate acceleration. Indeed, as $\gamma \to \infty$, irrespective of the form of the surface profile, the wall velocity tends to a constant value.

By appropriately scaling the streamwise and wall-normal velocity components one finds

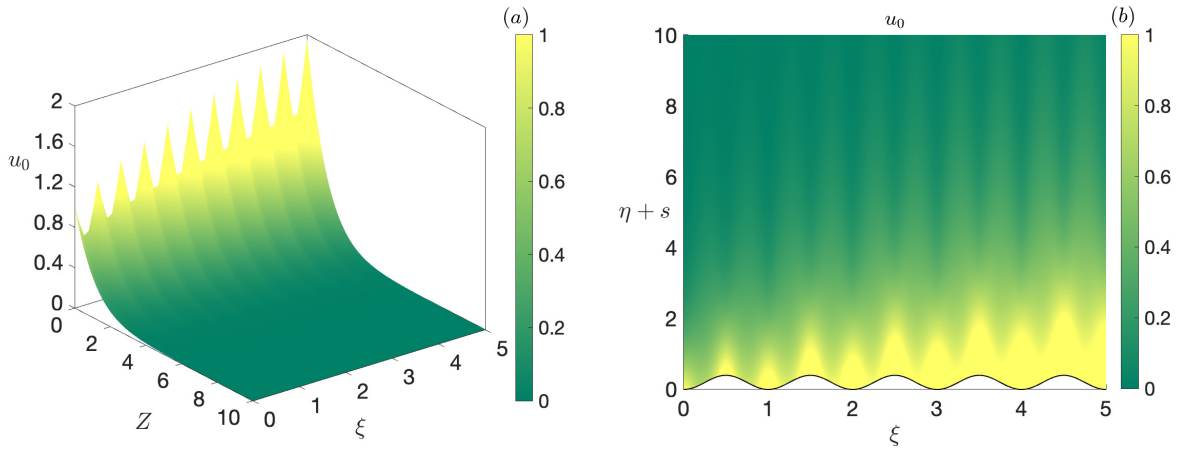


FIG. 7. In (a) a 3D-plot of the streamwise velocity $u_0$ against $\xi$ and $Z$. In (b) the solution for $u_0$ has been mapped back to the unscaled boundary layer coordinate system $(\xi, \eta + s)$. In both plots the roughness parameter, $\varepsilon$, has been set equal to one-fifth; the initial wall velocity, ${}_0U_w$, is set equal to 1; and the surface is moderately accelerating with $\gamma = 2$. In (b) the solid black line indicates the surface of the rough sheet.

that the velocity profiles are cyclical in nature and have the following properties:

$$(U_0, V_0) = \begin{cases} \left(\hat{f}'_Z, \sqrt{\dfrac{1}{2\alpha}}\left(\dfrac{\gamma}{(2+\gamma)} Z \hat{f}'_Z - \hat{f}\right)\right), & \text{when} \quad \xi = \dfrac{(n-1)}{2}, \\ \left(\dfrac{\hat{f}'_Z}{\sqrt{1+(2\varepsilon\pi)^2}}, \sqrt{\dfrac{1+(2\varepsilon\pi)^2}{2\alpha}}\left(\dfrac{\gamma}{(2+\gamma)} Z \hat{f}'_Z - \hat{f}\right)\right), & \text{when} \quad \xi = \dfrac{(n-\frac{1}{2})}{2}, \end{cases}$$

for $n = 1, 2, 3, \ldots$, with $U_0 = u_0/U_w$, and $V_0 = U_w^{\gamma/2} v_0$. These self-similar flow profiles are depicted in Fig. 6 where we observe that at the points where $|s'_\xi|$ is at a maximum, i.e., when $2\xi = (n - \frac{1}{2})$, the value of the streamwise velocity at the wall decreases to a minimum. In order to compensate for this, the magnitude of the vertical velocity component at the far-field attains a maximum value at these points. Given that no exact analytical solution for $\hat{f}$ exists in the case when $\gamma = 2$, a shooting method that makes use of a fourth-order Runge-Kutta integrator, twinned with a secant root finding scheme, was employed to solve (14).

In order to better visualise the downstream development of the streamwise velocity component, $u_0$, we plot, in Fig. 7, the flow in both the scaled $(\xi, Z)$, and unscaled $(\xi, \eta + s)$ coordinates systems. The sinusoidal nature of the surface roughness profile is evidenced in

the development of the streamwise flow where we observe that the velocity attains local maximums at the respective locations of maximum roughness amplitude.

The solutions presented within this subsection serve to highlight how our formulation can be used to model flows developing over small amplitude rough surfaces. Indeed, this analysis could readily be extended to incorporate a random surface roughness model whereby the function $s(\xi)$ is defined, for example, via a Fourier series composed of a randomised phase spectrum as per the work of Lu *et al.*[18].

### D. Numerical Validation

The primary motivation for this study is the determination of boundary-layer flows induced by stretching surfaces, as presented in Sec. III A. As such, we chose to validate the analytical solutions presented in Fig. 4 for the case of an exponentially thinning sheet against a suitable numerical scheme. To solve the governing system of PDEs numerically we use the finite element software FEniCS (Logg, Mardal, and Wells[19]). It is convenient to rewrite our equations in terms of the the divergence of the stress tensor $\boldsymbol{\tau}^*$, such that

$$\boldsymbol{\nabla}^* \cdot \mathbf{u}^* = 0, \tag{15a}$$

$$\rho^*(\mathbf{u}^* \cdot \boldsymbol{\nabla}^*)\mathbf{u}^* = \boldsymbol{\nabla}^* \cdot \boldsymbol{\tau}^*. \tag{15b}$$

We apply the same coordinate system transformation and nondimensionalisation as before, with the exception that we scale the pressure by a factor of $\mathrm{Re}^{1/2}$. This difference in the pressure scale can be attained by referring to (4c), where it is seen that the pressure term is $\mathcal{O}(\mathrm{Re}^{1/2})$ larger than the next largest term in the $\eta$-momentum equation. This fact, twinned with the free stream boundary condition, $U_\infty = 0$, allowed us to deduce that pressure in the boundary layer was constant to leading order. However, rescaling our pressure as $p \sim \mathrm{Re}^{-1/2}$ allows the pressure to vary and results in us being able to numerically determine the non-constant pressure correction. Note that this is in contrast to the corresponding flat stretching sheet analysis of Crane[4] where $p \sim \mathrm{Re}^{-1}$, which would be the case in (4c) if $s'_\xi = 0$. Thus,

we have that

$$\frac{\partial u}{\partial \xi} + \frac{\partial v}{\partial \eta} = 0, \tag{16a}$$

$$u\frac{\partial u}{\partial \xi} + v\frac{\partial u}{\partial \eta} = \left\{ \frac{\partial}{\partial \xi} - \mathrm{Re}^{1/2}\, s'_\xi \frac{\partial}{\partial \eta} \right\} \tau_{\xi\xi} + \mathrm{Re}^{1/2}\, \frac{\partial}{\partial \eta} \tau_{\xi\eta}, \tag{16b}$$

$$\begin{aligned} \mathrm{Re}^{-1/2} \left( u\frac{\partial v}{\partial \xi} + v\frac{\partial v}{\partial \eta} \right) = & -s'_\xi \left( u\frac{\partial u}{\partial \xi} + v\frac{\partial u}{\partial \eta} \right) - s''_{\xi\xi} u^2 \\ & + \mathrm{Re}^{-1} \left\{ \frac{\partial}{\partial \xi} - \mathrm{Re}^{1/2}\, s'_\xi \frac{\partial}{\partial \eta} \right\} \tau_{\xi\eta} + \mathrm{Re}^{1/2}\, \frac{\partial}{\partial \eta} \tau_{\eta\eta}, \end{aligned} \tag{16c}$$

where the components of the stress tensor are given by

$$\tau_{\xi\xi} = -\,\mathrm{Re}^{-1/2}\, p + 2\,\mathrm{Re}^{-1} \left( \frac{\partial u}{\partial \xi} - \mathrm{Re}^{1/2}\, s'_\xi \frac{\partial u}{\partial \eta} \right), \tag{16d}$$

$$\tau_{\xi\eta} = +\,\mathrm{Re}^{-1} \left\{ \mathrm{Re}^{1/2} [1 - (s'_\xi)^2] \frac{\partial u}{\partial \eta} + \mathrm{Re}^{-1/2}\, \frac{\partial v}{\partial \xi} + s'_\xi \left( \frac{\partial u}{\partial \xi} - \frac{\partial v}{\partial \eta} \right) + s''_{\xi\xi} u \right\}, \tag{16e}$$

$$\tau_{\eta\eta} = -\,\mathrm{Re}^{-1/2}\, p + 2\,\mathrm{Re}^{-1} \left( \frac{\partial v}{\partial \eta} + \mathrm{Re}^{1/2}\, s'_\xi \frac{\partial u}{\partial \eta} \right). \tag{16f}$$

System (16) is then solved subject to the following boundary conditions:

$$u = u_0, \quad v = v_0, \quad \text{at} \quad \xi = 0 \quad \text{and} \quad \xi = \xi_\infty, \tag{17a}$$

$$u = U_w/\sigma, \quad v = 0, \quad \text{at} \quad \eta = 0, \tag{17b}$$

$$u = 0, \quad \boldsymbol{\tau} \cdot \boldsymbol{n} = 0, \quad \text{at} \quad \eta = \eta_\infty. \tag{17c}$$

We apply our normal and tangential velocity conditions at the wall and the condition that the streamwise velocity component decays in the far-field, as per the solution of our boundary layer equations (6). In solving the full Navier-Stokes equations we need to impose additional constraints on the system. Here we use our boundary-layer solutions as inlet and outlet conditions. We also impose a no stress condition at the outlet. This choice of free stream condition allows us to measure convergence by means of evaluation of the wall-normal velocity component at the far-field, $v_0|_{\eta=\eta_\infty}$, for any fixed $\xi$, since we have not explicitly forced this value. Indeed, this can be seen in Fig. 8, where the difference in the absolute value between the boundary-layer and numerical wall-normal velocity solutions decrease as the Reynolds number grows larger. In the transformed coordinates our boundary-layer solutions are given by

$$\begin{aligned} u_0 &= \frac{U_w}{\sigma}\, \mathrm{e}^{-\eta/\sigma}, \\ v_0 &= \frac{U_w \sigma'_\xi}{\sigma^2} \eta\, \mathrm{e}^{-\eta/\sigma} - (U_w)'_\xi (1 - \mathrm{e}^{-\eta/\sigma}). \end{aligned}$$

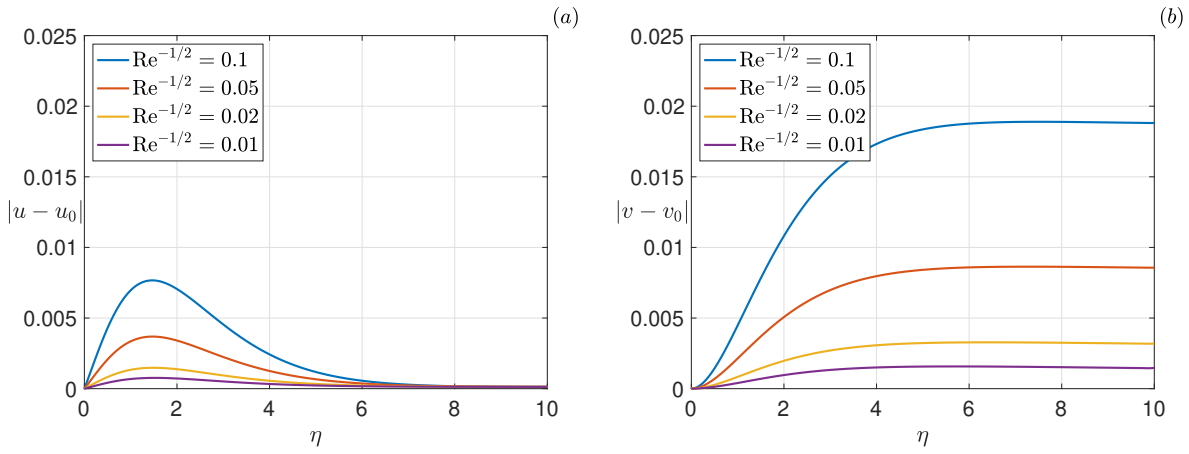


FIG. 8. In (a) we plot the absolute value of the difference between the numerical solutions for the streamwise velocity component at $\xi = 2.5$, with the corresponding boundary-layer solution at the same point, for a range of values of the small parameter $\mathrm{Re}^{-1/2}$. In (b) we plot an identical comparison for the wall-normal velocity component.

It is these solutions that we compare, respectively, to the numerical results for $u$ and $v$. The domain $[\xi, \eta] \in [0, 5] \times [0, 10]$ was triangulated using a $200 \times 200$ mesh with the originally uniformly spaced mesh mapped via

$$\eta_{\mathrm{new}} = \eta \frac{\exp\left(\eta/\eta_\infty\right) - 1}{\exp(1) - 1},$$

to accurately resolve the boundary layer near the surface of the sheet. To ensure the mesh was properly resolved the problem was also solved on a $100 \times 100$ and $50 \times 50$ mesh, with $|v - v_0|_{\eta=\eta_\infty}$, at $\xi = 2.5$, being used to measure the errors for a range of different mesh densities and Reynolds numbers. The errors were determined to be a function of the size of the Reynolds number with the mesh density playing almost no role at all, giving us confidence that our mesh is sufficiently refined.

The choice of $\eta_\infty$ was further validated by solving the problem on incrementally larger domains, where it was found that $\eta_\infty = 10$, was appropriate provided the Reynolds number was sufficiently large. Plots comparing the difference between our self-similar and finite element solutions are presented in Fig. 8 for a range of Reynolds numbers. Given that our boundary-layer analysis hinges on an asymptotic expansion with small parameter $\mathrm{Re}^{-1/2}$, it is logical for us to present results for a range of values of this small quantity. As expected we observe that the difference between the large Reynolds number analytical solutions and

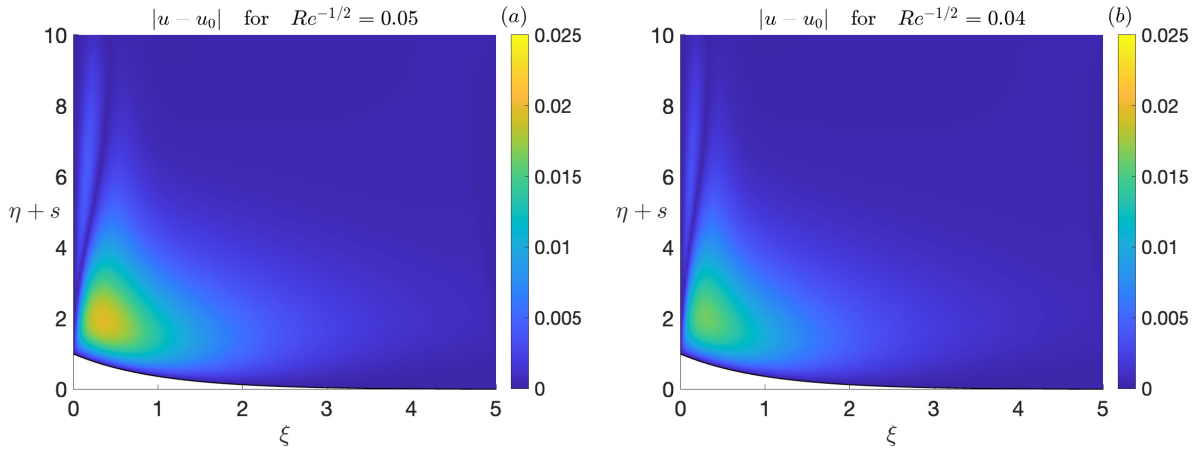


FIG. 9. Comparison between the finite element and boundary-layer solutions across the computational domain for (a) $\mathrm{Re}^{-1/2} = 0.05$ and (b) $\mathrm{Re}^{-1/2} = 0.04$. The same colourbar scale is used in both instances so that the reduction in error may be easily observed.

the numerical solutions decreases as the Reynolds number increases.

In Fig. 9 we present a comparison of the boundary-layer and finite element solution for the streamwise velocity component across the entire $(\xi, \eta + s)$ domain. It is clear that our analytical boundary-layer solutions provide an excellent approximation to the full numerical solutions. Indeed, upon decreasing our small parameter $\mathrm{Re}^{-1/2}$, one observes a notable decrease in the absolute difference between the two sets of solutions.

## IV. DISCUSSION AND CONCLUSIONS

We have shown that it is possible to obtain self-similar boundary-layer solutions over deforming surfaces and have investigated a number of specific case studies. Our analysis is primarily focused on flows that are generated from extrusion-type processes, whereby surfaces accelerate and thin as they are extruded. The vast majority of studies in the literature fail to account for this surface curvature and instead assume that the sheet is flat, following the analysis of Crane[4]. We show that in order to accurately describe boundary layer flows over stretching surfaces one needs to account for the curvature of the surface. Failing to do so results in incorrect predictions for both the streamwise and wall-normal velocity components. Most notably, near to the extrusion inlet, we find that the magnitude of the wall-normal velocity at the far-field is significantly increased when compared to the

corresponding flat-plate results. Our analytical results have been verified numerically using an appropriate finite element scheme and we observe excellent agreement between the two sets of solutions.

Our formulation has been shown to be general enough that it can be extended to consider both flows over thickening, decelerating surfaces and also the development of boundary-layer flows over periodic rough surfaces. Our analysis stipulates that the exact form of the wall velocity is dictated by the shape of the deforming surface. However, we have shown that, at least for the case studies considered here, these expressions for the wall velocity can be very well approximated by simple expressions involving only the streamwise coordinate $\xi$. In practice, one would measure the velocity of the deforming sheet and stipulate the value of the constant $\gamma$ to ensure that the predicted wall velocity closely matched experimental observations, and, indeed, our analysis allows for exactly this procedure. Our analysis could easily be extended to consider other types of flows generated from extrusion processes including those over bounded domains. In these cases, one would replace the analytical calculation the arc length of the surface, $\mathcal{I}$, with a numerical integration scheme with the limits of integration dictated by the bounds of the domain.

In a sense the current study is somewhat related that of Crane [20], where similarity solutions for the boundary-layer flow induced by a stretching cylinder were derived. However, these solutions are only valid when the ratio of cross-sectional areas of the boundary layer to the cylinder is large. Both the velocity and shape of the cylinder are prescribed in a manner that ensures that mass is conserved within the cylinder i.e., the density is constant. In much the same way as the corresponding flat plate study[4] the cylinder wall is not treated as a deformable quantity. The approach we have presented here would be capable of describing more general boundary-layer solutions in other such non-Cartesian geometries, and, as such, could remove the limitations of the studies relating to flows induced by stretching cylinders.

Recent research has shown that Crane's flow is linearly stable to Görtler type disturbances (Davis and Pozrikidis [21]) but is linearly unstable to Tollmien-Schlichting (TS) type disturbances (Griffiths, Stephen, and Khan [22]). However, both analyses centre on the fact that the sheet is not deformed as it is stretched. Given that we have shown that the basic flow solutions are significantly altered when surface deformation is accounted for, it would seem natural to re-pose questions regarding the linear stability of these types of flows to either non-propagating (Görtler) or propagating (TS) disturbances. Indeed, we are currently

pursuing this avenue of investigation and hope to report on this in due course.


## ACKNOWLEDGMENTS

We wish to acknowledge the insights provided by both Dr. Liam Escott and Dr. Sharon Stephen. Their useful comments no doubt improved the overall quality of this manuscript.


## DATA AVAILABILITY STATEMENT

The data that support the findings of this study are available from the corresponding author upon reasonable request.

## Appendix A: Self-similar solutions in the limit as $c_i \to 0$

In the first instance we consider the case when $c_1 = 0$. This is directly equivalent to the case when $\gamma = -2$. From (7a) it is immediately apparent that if $c_1 = 0$, then it must be the case that $X_+ = 0$. Solving this resulting ODE we determine that $g = k\sqrt{(\xi U_w)^{-1}\sigma}$, where $k$ is a constant of integration. Thus from (7b) it follows that $U_w = -c_2^{-1}k^2\mathcal{I}^{-1}$. Given that we consider only cases where the wall velocity is positive we fix $c_2 = -k^2$. Now, by writing $\hat{f}(Z) = kf(\zeta) = \psi$, where $Z = k\zeta = \sigma^{-1}\eta U_w$, we have that $u_0 = \sigma^{-1}U_w\hat{f}'_Z$, and $v_0 = Z\hat{f}'_Z[\sigma^{-1}\sigma'_\xi - U_w^{-1}(U_w)'_\xi]$. The ODE that governs the flow is then

$$\hat{f}'''_{ZZZ} + (\hat{f}'_Z)^2 = 0,$$

which must be solved subject to

$$\hat{f}(0) = 0, \quad \hat{f}'_Z(0) = 1, \quad \hat{f}'_Z(\infty) = 0.$$

The ODE in question can be integrated to give

$$\frac{1}{2}(\hat{f}''_{ZZ})^2 + \frac{1}{3}(\hat{f}'_Z)^3 = 0.$$

The right-hand side of the above must be equal to zero to ensure that the far-field condition is satisfied. In the limit as $Z \to 0$ it then follows that

$$\frac{1}{2}[\hat{f}''_{ZZ}(0)]^2 = -\frac{1}{3}.$$

Clearly, this cannot be true and, as such, we determine that no real solutions exist in the case when $\gamma = -2$ ($c_1 = 0$). This result is analogous to that associated with the Falkner-Skan problem in the limit as $m \to -1$. In that case one is unable to determine the flow in a diverging channel due to the very rapid deceleration of the free-stream velocity. We interpret our result in much the same way, given that $U_w$ is inversely proportional to $\mathcal{I}$ we conclude that the rapid change of the wall velocity to zero is such that a boundary-layer cannot be accommodated by this analysis.

In the second instance we consider the case when $c_2 = 0$. This is directly equivalent to the case when $\gamma \to \infty$. From (7b) it is immediately apparent that if $c_2 = 0$, then it must be the case that $U_w =$ constant. Given this result we determine, from (7a), that $g = k\sqrt{\xi^{-1}\mathcal{J}\sigma}$, where $k$ is a constant of integration fixed such that $2c_1 = k^2$, and $\mathcal{J} = C + \mathcal{I}$. Now, by writing $\hat{f}(Z) = kf(\zeta) = \psi/\sqrt{\mathcal{J}U_w}$, where $Z = k\zeta = \sigma^{-1}\eta\sqrt{\mathcal{J}^{-1}U_w}$ we have that $u_0 = \sigma^{-1}U_w\hat{f}'_Z$, and

$$v_0 = \frac{\sigma}{2}\sqrt{\frac{U_w}{\mathcal{J}}}\left\{\left[\frac{2\mathcal{J}\sigma'_\xi}{\sigma^2} + 1\right]Z\hat{f}'_Z - \hat{f}\right\}.$$

The ODE that governs the flow is then

$$\hat{f}'''_{ZZZ} + \frac{\hat{f}\hat{f}''_{ZZ}}{2} = 0,$$

which must be solved subject to

$$\hat{f}(0) = 0, \quad \hat{f}'_Z(0) = 1, \quad \hat{f}'_Z(\infty) = 0.$$

The above ODE and boundary conditions are identical to those presented by Tsou, Sparrow, and Kurtz[13] who considered purely the case when $s(\xi) = 0$. Thus, in all cases when the wall velocity is constant, the boundary-layer flow over non-flat surfaces can be determined from the solutions associated with the flow over a flat smooth boundary.

There is a special case to consider when $\sigma/\sqrt{\mathcal{J}} = d_1 =$ constant. In this case $v_0$ is a function of $Z$ only. It follows that

$$\sigma = \frac{d_1}{2}(d_2 + d_1\xi),$$

where $C = d_2^2/4$. Stipulating that $s_0 = 0$, and fixing $d_1/2 = d_2 = 1$, gives

$$s(\xi) = \frac{\sigma\sqrt{\mathcal{I}}}{2} - \frac{1}{2}\ln\left(\sqrt{\frac{\sigma-1}{2}} + \sqrt{\frac{\sigma+1}{2}}\right).$$

Then $\sigma u_0/U_w = \hat{f}'_Z$, and $v_0/\sqrt{U_w} = (2Z\hat{f}'_Z - \hat{f})$.

## Appendix B: Derivation of the exact solutions

Consider equation (14). For convenience we define $q = 2/(2+\gamma)$ so that now we seek solutions to

$$\hat{f}'''_{ZZZ} + \hat{f}\hat{f}''_{ZZ} - q(\hat{f}'_Z)^2 = 0,$$

subject to

$$\hat{f}(0) = 0, \quad \hat{f}'_Z(0) = 1, \quad \hat{f}'_Z(\infty) = 0.$$

Following the same approach as Sachdev, Bujurke, and Pai [15] we suppose that

$$\hat{f}(Z) = b + b\sum_{n=1}^{\infty} A^n \hat{a}_n \, \mathrm{e}^{-bnZ} \quad \text{where} \quad A = \frac{a_1}{b} \quad \text{and} \quad \hat{a}_1 = 1. \tag{B1}$$

The constants $a_1$, $\hat{a}_n$ and $b$ need to be determined. Note $\hat{f}'_Z(\infty) = 0$ is already satisfied. Substituting this expression for $\hat{f}$ into the ODE gives

$$\sum_{n=2}^{\infty} A^n \mathrm{e}^{-bnZ} \left( -\hat{a}_n n^2(n-1) + \sum_{j=1}^{n-1} \hat{a}_j \hat{a}_{n-j}(n-j)[n-(q+1)j] \right) = 0.$$

To satisfy this we require that

$$\hat{a}_n = \frac{1}{n^2(n-1)} \sum_{j=1}^{n-1} \hat{a}_j \hat{a}_{n-j}(n-j)[n-(q+1)j] \quad \text{for} \quad n \geq 2. \tag{B2}$$

The first few values are given by

$$\begin{aligned} \hat{a}_2 &= \frac{1-q}{4}, \qquad \hat{a}_3 = \frac{1-q}{72}(5-4q), \qquad \hat{a}_4 = \frac{1-q}{1728}(34-53q+21q^2), \\ \hat{a}_5 &= \frac{1-q}{172800}(968-2235q+1741q^2-456q^3), \qquad \ldots. \end{aligned}$$

Using $\hat{f}(0) = 0$ we obtain

$$\sum_{n=1}^{\infty} A^n \hat{a}_n = -1, \tag{B3}$$

which is a polynomial in the unknown $A$. By truncating this to a finite series we can numerically obtain the value of $A$. The condition $\hat{f}'_Z(0) = 1$ yields

$$b = \frac{1}{\sqrt{-\sum_{n=1}^{\infty} n\hat{a}_n A^n}}. \tag{B4}$$

With $A$ and $b$ known, we can determine $a_1$ using $a_1 = Ab$.

**Special case:** $q = 1$

If $q = 1$, then $\hat{a}_n = 0$ for $n \geq 2$ and therefore

$$\hat{f}(Z) = b + a_1 \, \mathrm{e}^{-bZ}.$$

Applying our boundary conditions yields $a_1 = b = 1$. Hence

$$\hat{f}(Z) = 1 + \mathrm{e}^{-Z}.$$

**Special case:** $q = -1$

If $q = -1$, then equation (B2) reduces to

$$\hat{a}_n = \frac{1}{n(n-1)} \sum_{j=1}^{n-1} \hat{a}_j \hat{a}_{n-j} (n-j) \quad \text{for} \quad n \geq 2.$$

With $\hat{a}_1 = 1$, the solution is given by $\hat{a}_n = 2^{1-n}$. Thus one finds that

$$\hat{f}(Z) \; = \; b + 2b \sum_{n=1}^{\infty} \left( \frac{A}{2} \, \mathrm{e}^{-bZ} \right)^n = b \frac{2 + A\mathrm{e}^{-bZ}}{2 - A\mathrm{e}^{-bZ}}.$$

Substituting this solution into $\hat{f}(0) = 0$ gives $A = -2$. Further $\hat{f}'_Z(0) = 1$ gives $b^2 = 2$, and hence

$$\hat{f}(Z) = \sqrt{2} \frac{1 - \mathrm{e}^{-\sqrt{2}Z}}{1 + \mathrm{e}^{-\sqrt{2}Z}} = \sqrt{2} \tanh\left( \frac{Z}{\sqrt{2}} \right).$$

## REFERENCES


[1]F. T. Trouton, "On the coefficient of viscous traction and its relation to that of viscosity," Proc. R. Soc. Lond. A **77**, 426–440 (1906).

[2]P. D. Howell, "Models for thin viscous sheets," Eur. J. App. Math. **7**, 321–343 (1996).

[3]J. R. A. Pearson and M. A. Matovich, "Spinning a molten threadline. Stability," Ind. Eng. Chem. Fundamen. **8**, 605–609 (1969).

[4]L. J. Crane, "Flow past a stretching plate," Z. fur Angew. Math. Phys. **21**, 645–647 (1970).

[5]S. N. Bhattacharyya and A. S. Gupta, "On the stability of viscous flow over a stretching sheet," Q. Appl. Math. **43**, 359–367 (1985).

[6]T. T. Al-Housseiny and H. A. Stone, "On boundary-layer flows induced by the motion of stretching surfaces," J. Fluid Mech. **706**, 597–606 (2012).

[7]D. A. S. Rees and I. Pop, "Boundary layer flow and heat transfer on a continuous moving wavy surface," Acta. Mech. **112**, 149–158 (1995).

[8]M. S. Yoon, J. M. Hyun, and J. S. Park, "Flow and heat transfer over a rotating disk with surface roughness," Int. J. Heat Fluid Flow **28**, 262–267 (2007).

[9]S. J. Garrett, A. J. Cooper, J. H. Harris, M. Özkan, A. Segalini, and P. J. Thomas, "On the stability of von Kármán rotating-disk boundary layers with radial anisotropic surface roughness," Phys. Fluids **28**, 014104 (2016).

[10]S. Bickerton, M. J. Buntain, and A. A. Somashekar, "The viscoelastic compression behavior of liquid composite molding preforms," Compos. Part A Appl. Sci. Manuf. **34**, 431–444 (2003).

[11]P. A. Kelly, "A viscoelastic model for the compaction of fibrous materials," J. Text. Inst. **102**, 689–699 (2011).

[12]I. Pop and S. Nakamura, "Laminar boundary layer flow of power-law fluids over wavy surfaces," Acta Mech. **115**, 55–65 (1996).

[13]F. K. Tsou, E. M. Sparrow, and E. F. Kurtz, "Hydrodynamic stability of the boundary layer on a continuous moving surfaces," J. Fluid Mech. **26**, 145–161 (1966).

[14]J. A. D. Ackroyd, "A series method for the solution of laminar boundary layers on moving surfaces," Z. fur Angew. Math. Phys. **29**, 729–741 (1978).

[15]P. L. Sachdev, N. M. Bujurke, and N. P. Pai, "Dirichlet series solution of equations arising in boundary layer theory," Math. Comput. Model. **32**, 971–980 (2000).

[16]A. J. Thompson, J. R. McFarlane, J. P.-H. Belnoue, and S. R. Hallett, "Numerical modelling of compaction induced defects in thick 2d textile composites," Mater. Des. **196**, 109088 (2020).

[17]M. Abramowitz and I. A. Stegun, "Handbook of Mathematical Functions," (Dover Publications, New York, 1972) pp. 555–566.

[18]H. Lu, M. Xu, L. Gong, X. Duan, and J. C. Chai, "Effects of surface roughness in microchannel with passive heat transfer enhancement structures," Int. J. Heat Mass Transf. **148**, 119070 (2020).

[19]A. Logg, K.-A. Mardal, and G. Wells, *Automated Solution of Differential Equations by the Finite Element Method: The FEniCS book*, Vol. 84 (Springer Science & Business Media, 2012).

[20]L. J. Crane, "Boundary layer flow due to a stretching cylinder," Z. fur Angew. Math. Phys. **26**, 619–622 (1975).

[21]J. M. Davis and C. Pozrikidis, "Linear stability of viscous flow induced by surface stretching," Arch. Appl. Mech. **84**, 985–998 (2014).

[22]P. T. Griffiths, S. O. Stephen, and M. Khan, "Stability of the flow due to a linear stretching sheet," Phys. Fluids **33**, 084106 (2021).